Results of the search for inspiraling compact star binaries from TAMA300's observation in 2000–2004

Tomomi Akutsu,[1] Tomotada Akutsu,[2] Masaki Ando,[3] Koji Arai,[4] Akito Araya,[5] Hideki Asada,[6] Youichi Aso,[3]
Mark A. Barton,[1] Peter Beyersdorf,[4] Youhei Fujiki,[7] Masa-Katsu Fujimoto,[4] Ryuichi Fujita,[8] Mitsuhiro Fukushima,[4]
Toshifumi Futamase,[9] Yusaku Hamuro,[7] Tomiyoshi Haruyama,[10] Hideaki Hayakawa,[1] Kazuhiro Hayama,[2,*]
Gerhard Heinzel,[11] Gen'ichi Horikoshi,[10,†] Hideo Iguchi,[12] Yukiyoshi Iida,[3] Kunihito Ioka,[13] Hideki Ishitsuka,[1]
Norihiko Kamikubota,[10] Nobuyuki Kanda,[14] Takaharu Kaneyama,[7] Yoshikazu Karasawa,[9] Kunihiko Kasahara,[1]
Taketoshi Kasai,[6] Mayu Katsuki,[14] Keita Kawabe,[15] Mari Kawamura,[16] Seiji Kawamura,[4] Nobuki Kawashima,[17]
Fumiko Kawazoe,[18] Yasufumi Kojima,[19] Keiko Kokeyama,[18] Kazuhiro Kondo,[1] Yoshihide Kozai,[4] Hideaki Kudoh,[20]
Kazuaki Kuroda,[1] Takashi Kuwabara,[7] Namio Matsuda,[21] Norikatsu Mio,[22] Kazuyuki Miura,[23] Osamu Miyakawa,[24]
Shoken Miyama,[4] Shinji Miyoki,[1] Hiromi Mizusawa,[7] Shigenori Moriwaki,[22] Mitsuru Musha,[25] Shigeo Nagano,[26]
Yoshitaka Nagayama,[14] Ken'ichi Nakagawa,[25] Takashi Nakamura,[16] Hiroyuki Nakano,[14,*] Ken-ichi Nakao,[14]
Yuhiko Nishi,[3] Kenji Numata,[27] Yujiro Ogawa,[10] Masatake Ohashi,[1] Naoko Ohishi,[4] Akira Okutomi,[1] Ken-ichi Oohara,[7]
Shigemi Otsuka,[3] Norichika Sago,[8,‡] Yoshio Saito,[10] Shihori Sakata,[18] Misao Sasaki,[28] Kouichi Sato,[29] Nobuaki Sato,[10]
Shuichi Sato,[4] Youhei Sato,[25] Hidetsugu Seki,[3] Aya Sekido,[30] Naoki Seto,[31] Masaru Shibata,[32] Hisaaki Shinkai,[33]
Takakazu Shintomi,[10] Kenji Soida,[3] Kentaro Somiya,[34] Toshikazu Suzuki,[10] Hideyuki Tagoshi,[8] Hirotaka Takahashi,[34]
Ryutaro Takahashi,[4] Akiteru Takamori,[5] Shuzo Takemoto,[16] Kohei Takeno,[22] Takahiro Tanaka,[16] Keisuke Taniguchi,[35]
Shinsuke Taniguchi,[3] Toru Tanji,[22] Daisuke Tatsumi,[4] C. T. Taylor,[1] Souichi Telada,[36] Kuniharu Tochikubo,[3]
Masao Tokunari,[1] Takayuki Tomaru,[10] Kimio Tsubono,[3] Nobuhiro Tsuda,[29] Yoshiki Tsunesada,[4] Takashi Uchiyama,[1]
Akitoshi Ueda,[4] Ken-ichi Ueda,[25] Fumihiko Usui,[37] Koichi Waseda,[4] Yuko Watanabe,[23] Hiromi Yakura,[23]
Akira Yamamoto,[10] Kazuhiro Yamamoto,[1] Toshitaka Yamazaki,[4] Yuriko Yanagi,[18] Tatsuo Yoda,[3] Jun'ichi Yokoyama,[38]
Tatsuru Yoshida,[9] and Zong-Hong Zhu[4]

(TAMA Collaboration)

[1]*Institute for Cosmic Ray Research, The University of Tokyo, Kashiwa, Chiba 277-8582, Japan*
[2]*Department of Astronomy, The University of Tokyo, Bunkyo-ku, Tokyo 113-0033, Japan*
[3]*Department of Physics, The University of Tokyo, Bunkyo-ku, Tokyo 113-0033, Japan*
[4]*National Astronomical Observatory, Mitaka, Tokyo 181-8588, Japan*
[5]*Earthquake Research Institute, The University of Tokyo, Bunkyo-ku, Tokyo 113-0032, Japan*
[6]*Faculty of Science and Technology, Hirosaki University, Hirosaki, Aomori 036-8561, Japan*
[7]*Faculty of Science, Niigata University, Niigata, Niigata 950-2102, Japan*
[8]*Graduate School of Science, Osaka University, Toyonaka, Osaka 560-0043, Japan*
[9]*Graduate School of Science, Tohoku University, Sendai, Miyagi 980-8578, Japan*
[10]*High Energy Accelerator Research Organization, Tsukuba, Ibaraki 305-0801, Japan*
[11]*Max-Planck-Institut für Gravitationsphysik, Callinstrasse 38, D-30167 Hannover, Germany*
[12]*Tokyo Institute of Technology, Meguro-ku, Tokyo 152-8551, Japan*
[13]*Physics Department, Pennsylvania State University, University Park, Pennsylvania 16802, USA*
[14]*Graduate School of Science, Osaka City University, Sumiyoshi-ku, Osaka 558-8585, Japan*
[15]*LIGO Hanford Observatory, Richland, Washington 99352, USA*
[16]*Faculty of Science, Kyoto University, Sakyo-ku, Kyoto 606-8502, Japan*
[17]*Kinki University, Higashi-Osaka, Osaka 577-8502, Japan*
[18]*Ochanomizu University, Bunkyo-ku, Tokyo 112-8610, Japan*
[19]*Department of Physics, Hiroshima University, Higashi-Hiroshima, Hiroshima 739-8526, Japan*
[20]*Theoretical Astrophysics Group, Department of Physics, The University of Tokyo, Bunkyo-ku, Tokyo 113-0033, Japan*
[21]*Tokyo Denki University, Chiyoda-ku, Tokyo 101-8457, Japan*
[22]*Department of Advanced Materials Science, The University of Tokyo, Kashiwa, Chiba 277-8561, Japan*
[23]*Department of Physics, Miyagi University of Education, Aoba Aramaki, Sendai 980-0845, Japan*
[24]*California Institute of Technology, Pasadena, California 91125, USA*
[25]*Institute for Laser Science, University of Electro-Communications, Chofugaoka, Chofu, Tokyo 182-8585, Japan*
[26]*National Institute of Information and Communications Technology, Koganei, Tokyo 184-8795, Japan*
[27]*NASA Goddard Space Flight Center, Greenbelt, Maryland 20771, USA*
[28]*Yukawa Institute for Theoretical Physics, Kyoto University, Sakyo-ku, Kyoto 606-8502, Japan*
[29]*Precision Engineering Division, Faculty of Engineering, Tokai University, Hiratsuka, Kanagawa 259-1292, Japan*
[30]*Waseda University, Shinjyuku-ku, Tokyo 169-8555, Japan*

[31]*Theoretical Astrophysics, California Institute of Technology, Pasadena, California 91125, USA*

[32]*Graduate School of Arts and Sciences, The University of Tokyo, Meguro-ku, Tokyo 153-8902, Japan*

[33]*Department of Information Science, Osaka Institute of Technology, Hirakata, Osaka 573-0196, Japan*

[34]*Max-Planck-Institut für Gravitationsphysik, Albert-Einstein-Institut, Am Mühlenberg 1, D-14476 Golm bei Potsdam, Germany*

[35]*Department of Physics, University of Illinois at Urbana-Champaign, Urbana, Illinois 61801-3080, USA*

[36]*National Institute of Advanced Industrial Science and Technology, Tsukuba, Ibaraki 305-8563, Japan*

[37]*ISAS/JAXA, Sagamihara, Kanagawa 229-8510, Japan*

[38]*Research Center for the Early Universe (RESCEU), Graduate School of Science, The University of Tokyo, Tokyo 113-0033, Japan*

We analyze the data of the TAMA300 detector to search for gravitational waves from inspiraling compact star binaries with masses of the component stars in the range $1M_\odot$–$3M_\odot$. In this analysis, 2705 hours of data, taken during the years 2000–2004, are used for the event search. We combine the results of different observation runs, and obtain a single upper limit on the rate of the coalescence of compact binaries in our Galaxy of 20 per year at a 90% confidence level. In this upper limit, the effects of various systematic errors such as the uncertainty of the background estimation and the calibration of the detector's sensitivity are included.

I. INTRODUCTION

Several laser interferometric gravitational wave detectors of the first generation have been operated to detect gravitational waves. These include GEO [1], LIGO [2], TAMA300 [3], and VIRGO [4]. The sensitivity of these detectors has improved very rapidly in the past several years. The direct detection of gravitational waves is important not only because it will become a new astronomical tool to observe our Universe, but also because it will become a new tool to test general relativity and other gravity theories in a strong gravity field region.

In this paper, we present results of the data analysis of the TAMA300 detector to search for gravitational waves produced by inspiraling compact star binaries, comprised of nonspinning neutron stars and/or black holes. Inspiraling compact binaries are considered to be one of the most promising sources for ground based laser interferometers. TAMA300 has performed nine observation runs since 1999. The total amount of data is more than 3000 hours. Given such a large amount of data, it is very interesting to analyze the data to search for gravitational wave event candidates and to set an upper limit on the event rate.

In the past, there were several works which searched for inspiraling compact binaries using laser interferometer data. Allen *et al.* [5] analyzed LIGO-40m's data in the mass range $1M_\odot$–$3M_\odot$, and obtained an upper limit of 0.5 (1/hour) on the Galactic event rate. The data from "Data Taking 2" (DT2) of TAMA300 in 1999 were analyzed in the mass range $0.3M_\odot$–$10M_\odot$ [6], and an upper limit of 0.59 (1/hour) on the event rate with a signal-to-noise ratio greater than 7.2 was obtained. TAMA300's DT6 data and LISM-20m's data taken in 2001 were analyzed to search for coincident signals, and an upper limit of 0.046 (1/hour) on the nearby event rate within 1 kpc from the Earth was obtained [7]. Abbott *et al.* [8] analyzed LIGO's "1st science run" (S1) data taken in 2002, and obtained an upper limit of 1.7×10^2 per year per Milky Way equivalent galaxy (MWEG) in the mass range $1M_\odot$–$3M_\odot$. Abbott *et al.* analyzed LIGO S2 data taken in 2003, and obtained an upper limit of 47 per year per MWEG in the mass range $1M_\odot$–$3M_\odot$ [9], and 63 per year per Milky Way halo in the mass range $0.2M_\odot$–$1M_\odot$ [10]. LIGO's S2 data were also analyzed to search for binary black hole inspirals in the mass range $3M_\odot$–$20M_\odot$, and an upper limit of 37 per year per MWEG was obtained [11]. LIGO's S2 data and TAMA300's DT8 data were analyzed to search for coincident signals and an upper limit of 49 per year per MWEG was obtained [12]. In all of the above cases, there were no signals that could be identified as gravitational waves.

In this paper, we analyze the data from DT4, DT5, DT6, DT8, and DT9 of TAMA300. A part of DT6 data which was coincident with LISM was already analyzed in [7]. The initial results of the analysis of DT8 data were reported in Ref. [13]. Part of DT8 data which was coincident with LIGO S2 was already analyzed in [12]. In this paper, we analyze these data again, together with the other data in a unified way. Until the DT6 observation, TAMA300 was the only large scale laser interferometer which was operated. Thus, it is important to analyze such data to search for possible gravitational wave signals. Further, in order to take advantage of the long length of data from DT6, DT8, and DT9, we combine the results from the data and obtain a single upper limit on the rate of the coalescence of compact binaries in our Galaxy. We also evaluate the systematic errors caused by the uncertainty of the calibration and the background trigger rate. Other errors such as the uncertainty of the distribution model of sources and the uncertainty of the theoretical templates are also evaluated.

---

[*]Present address: Center for Gravitational Wave Astronomy, The University of Texas at Brownsville, 80 Fort Brown, Brownsville, TX 78520, USA.

[†]Deceased.

[‡]Present address: School of Mathematics, University of Southampton, Southampton SO17 1BJ, United Kingdom.

These systematic errors are taken into account to evaluate the upper limit.

This paper is organized as follows. In Sec. II, we give an overview of the detector and the data we analyze. In Sec. III, the analysis method is presented. In Sec. IV, the results of the analysis are presented. In Sec. V, the evaluation of the detection probability of the Galactic signals and the upper limit on the event rate are shown. In Sec. VI, we evaluate the errors due to various error sources and their effect on the upper limit. In Sec. VII, we summarize the results and present the conclusion.

II. DATA FROM THE TAMA300 DETECTOR

TAMA300 is a Fabry-Perot-Michelson interferometer with baseline length of 300 m located in Mitaka, Tokyo (35°40′N, 139°32′E). The history of the observation run of TAMA300 is listed in Table I. Until DT6, the detector was operated without the power recycling system. After DT6, the power recycling system was installed. The main signal of the detector is recorded with a 20 kHz, 16 bit data-acquisition system. There are more than 150 signals which monitor the condition and the environment of detector. During the operation, the mirrors of the detector are shaken by a 625 Hz sinusoidal signal in order to calibrate the detector sensitivity continuously.

We use DT4, DT5, DT6, DT8, and DT9 data of TAMA300. The observations of TAMA300 were interrupted by the unlocking of the detector. They were sometimes suspended manually for maintenance. By removing such dead time, the total length of data available for the data analysis is 3032 hours. Among them, we do not use the first 6.5 minutes of data just after the detector recovers from the dead time, because such data often contain signals due to the excitation of the violin modes of pendulum wires, and/or other signals caused by disturbance during the dead time. The data from the detector are converted into the strain equivalent data by applying the transfer function. The fluctuation of the transfer function at each

time is determined by computing the optical gain. We do not use the data if the value of the optical gain deviates from the average value significantly. The total amount of data remaining after removing such bad quality parts is 2705 hours. We analyze these data to search for gravitational wave events. However, we do not use DT4 and DT5 data to set the upper limit for the event rate, because the length of data from these runs is much shorter than DT6-8-9, and because the quality of data of these runs is much worse than DT6-8-9. The total amount of data used for setting the upper limit is 2462.8 hours.

III. ANALYSIS METHOD

The standard method to search for gravitational wave signals with known wave forms in noisy data is the matched filtering method, in which we search for the best matched parameters of the theoretical wave form by cross-correlating the data with the theoretical wave form. For the theoretical wave form, we use the nonspinning, restricted post-Newtonian (PN) wave form in which the phase is given to high post-Newtonian order, but only the leading quadrupole term is contained in the amplitude. We use the phase formula derived from the 2.5 PN approximation. Although the current best formula by the PN approximation is the 3.5 PN formula [14], the error due to the use of the 2.5 PN formula instead of the 3.5 PN formula is small for mass of binaries considered in this paper (see Sec. IV). On the other hand, the PN approximation itself may contain errors due mainly to the relativistic effects in the region when the orbital radius is the same order as the gravitational radius of stars. These effects will be incorporated in the systematic error to the detection probability of signals.

The basic formula of the matched filtering method is given by

$$\rho = \sqrt{(s, h_0)^2 + (s, h_{\pi/2})^2}, \tag{3.1}$$

TABLE I. Observation history of TAMA300. For each observation run, the period of the observation, the typical strain equivalent noise level around the most sensitive frequency region, the length of data observed, and the length of data analyzed in this paper are shown.

	Period	Typical strain noise $(1/\sqrt{Hz})$	Observed data (hours)	Analyzed data (hours)
DT1	6−7 Aug. 1999	3×10^{-19}	11	· · ·
DT2	17−20 Sept. 1999	3×10^{-20}	31	· · ·
DT3	20−23 April 2000	1×10^{-20}	13	· · ·
DT4	21 Aug.-4−Sept. 2000	1×10^{-20}	154.9	147.1
DT5	2−10 Mar. 2001	1.7×10^{-20}	107.8	95.26
DT6	1 Aug.−20 Sept. 2001	5×10^{-21}	1049	876.6
DT7	31 Aug.−2 Sept. 2002		25	· · ·
DT8	14 Feb.−14 April 2003	3×10^{-21}	1163	1100
DT9	28 Nov. 2003−10 Jan. 2004	1.5×10^{-21}	556.9	486.1
Total			3111.6	2705
(DT6, 8, 9 for upper limit)				(2462.8)

where

$$(a, b) \equiv 2 \int_{-\infty}^{\infty} \frac{\tilde{a}^*(f)\tilde{b}(f)}{S_n(|f|)} \, df, \qquad (3.2)$$

and where $\tilde{a}(f)$ and $\tilde{b}(f)$ are the Fourier transformation of time sequential data, $a(t)$ and $b(t)$. The Fourier transformation is defined by

$$\tilde{a}(f) = \int_{-\infty}^{\infty} a(t)e^{2\pi i f t} dt. \qquad (3.3)$$

The function $s(t)$ is the time sequential data from the detector. Two functions, h_0 and $h_{\pi/2}$, are the templates in the time domain, which are normalized as $(h_0, h_0) = (h_{\pi/2}, h_{\pi/2}) = 1$. The Fourier transformations of them, $\tilde{h}_0(f)$ and $\tilde{h}_{\pi/2}(f)$, are computed by the stationary phase approximation. We thus have the orthogonality of the functions, i.e., $(h_0, h_{\pi/2}) = 0$. The function $S_n(f)$ is the one-sided power spectrum density of noise of the detector.

The parameters which describe the wave form are the time of coalescence (t_c), the phase of the wave at coalescence (ϕ_c), the total mass $M \equiv m_1 + m_2$, and the non-dimensional reduced mass $\eta \equiv m_1 m_2/M^2$ of the binary. We search for the parameters which give the maximum of ρ. In the formula (3.1), the maximization over the phase is already taken analytically. The values of the parameters t_c, M, and η, which maximize ρ, are searched for numerically.

The data are divided into subsets of data with a length of 52.4 seconds. Each subset of data has overlapping data with adjacent data for 4.0 seconds. Each subset of data is Fourier transformed, and the components whose frequency is larger than 5 kHz are removed. The data are converted to the strain equivalent data $\tilde{s}(f)$ by the transfer function. The power spectrum density of noise of each subset of data is evaluated from the neighboring data. Details of the method to evaluate $S_n(f)$ were described in Sec. III.B of Ref. [7]. With the subset of data, we compute ρ. For each small time interval with length $\Delta t_c = 25.6$ msec, we search for t_c, M, and η which give the maximum of ρ. The value of ρ at all of t_c can be computed automatically from the inverse fast Fourier transform (FFT) of the inner product, Eq. (3.2), with respect to t_c. The search for the best matched M and η is done by introducing the grid points in the two dimensional mass parameter space. The range of masses of each member star of binaries is set to $1M_\odot$–$3M_\odot$. The grid separation length is determined so that the minimal match is less than 3% [15]. The actual mass parameters we use for setting up the mass parameter space are those discussed in [16]. We define *a trigger* by the local maximum of ρ in each small time interval with length $\Delta t_c = 25.6$ msec, and in the whole mass parameter region, together with the parameters t_c, M, and η which realize the local maximum.

IV. TRIGGER DISTRIBUTIONS

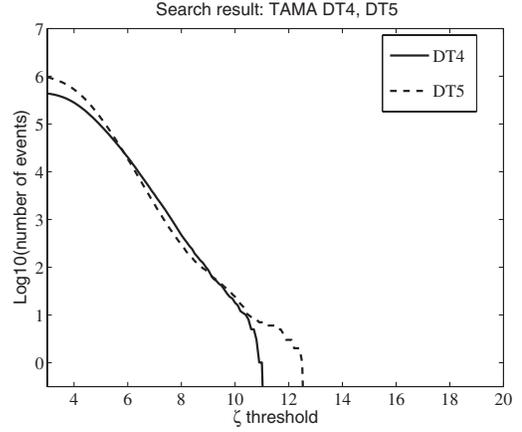The data of TAMA300 contain nonstationary, non-Gaussian noise. Such noise causes many triggers with a

FIG. 1.   The cumulative number of triggers as a function of ζ for DT4 and DT5.

rate much larger than that expected in the stationary Gaussian noise. In order to distinguish such spurious triggers from triggers caused by real gravitational wave signals, we compute the χ^2 value for each trigger with $\rho \gtrsim 7$. The definition of χ^2 can be found in [17,18]. This χ^2 is defined such that it is independent from the amplitude of the signal if the wave forms of the signal and the template are identical. However, since our template parameters are defined discretely, and thus the signals are different from the templates in general, when the amplitude of signal becomes larger, χ^2 becomes larger. In order not to lose real signals with large χ^2, we define $\zeta = \rho/\sqrt{\chi^2}$ as a new statistic [7]. The statistic ζ was used in our previous analysis [7], and was found to be useful to distinguish the spurious triggers from triggers caused by real gravitational wave signals.

The cumulative number distribution of triggers as a function of ζ for each observation run is plotted in Figs. 1 and 2.
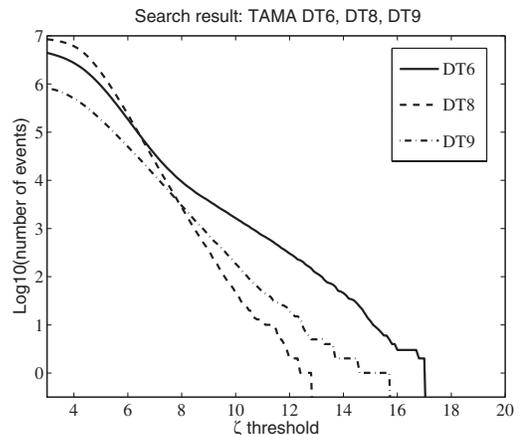

FIG. 2.   The cumulative number of triggers as a function of ζ for DT6, DT8, and DT9.

In these plots, there are no triggers which deviate from the tail of the distribution of triggers significantly. This fact suggests that there is no candidate trigger which can be interpreted as a real gravitational signal.

V. UPPER LIMIT ON THE GALACTIC EVENT RATE

In this section, we evaluate the upper limit on the rate of the inspirals of compact binaries in our Galaxy. In order to do this, we first evaluate the detection probability of Galactic signals by adding the signals to the real data, and by analyzing the data with the same analysis pipeline used in the real analysis. We assume the distribution of compact star binaries in our Galaxy given by

$$dN = e^{-r^2/(2r_0^2)} e^{-Z/h_z} r\,dr\,dZ, \qquad (5.1)$$

where r is the radius from the center of the Galaxy, $r_0 = 8.5$ kpc, Z is height from the Galactic plane, and $h_z = 1$ kpc. We assume that the mass of each component star is uniformly distributed between $1M_\odot$ and $3M_\odot$, because we do not know much about the mass distribution model of binary compact stars, including black holes and/or neutron stars. We also assume a uniformly distributed inclination angle of the orbital plane and the polarization angle of signals. The obtained detection probability is plotted in Fig. 3. DT9's data are the most sensitive to the Galactic events. Actually, the detection probability for the second half of the DT9 data is much better than that for the first half data. The first half of the data of DT9 was not very stable. Many triggers with large ζ were produced by instrumental noise during that period. They degrade the average detection probability in DT9.

The upper limit on the event rate from each observation run, R_i (i = DT6, DT8, DT9), is derived by

$$R_i = \frac{N_i}{T_i \epsilon_i}, \qquad (5.2)$$

where T_i is the length of data, ϵ_i is the detection probability, and N_i is the upper limit on the number of events derived by the following formula:

$$\frac{e^{-(N_i + N_{bg}^{(i)})} \sum_{n=0}^{n=N_{obs}^{(i)}} \frac{(N_i + N_{bg}^{(i)})^n}{n!}}{e^{-N_{bg}^{(i)}} \sum_{n=0}^{n=N_{obs}^{(i)}} \frac{(N_{bg}^{(i)})^n}{n!}} = 1 - \text{C.L.}, \qquad (5.3)$$

where $N_{obs}^{(i)}$ is the observed number of triggers which exceed a threshold, $N_{bg}^{(i)}$ is the number of triggers which are caused by noise alone, and C.L. is a confidence level.

We set the false alarm rate to 1 event per year. The threshold which corresponds to this false alarm rate is evaluated by fitting the trigger distribution assuming that all triggers are caused by noise. We note that $z \equiv \zeta^2/2$ obeys the F distribution with degree of freedom, $(2, 2p - 2)$, when the data are the Gaussian noise. Here, p is the number of bins in the frequency region which is used to define χ^2, and we set $p = 16$. In this case, the variable z obeys the probability density function given by $(p - 1)^p \times (z + p - 1)^{-p}$. The cumulative number of triggers as a function of the threshold, $N(z)$, is proportional to $N(z) \propto (p - 1)^{p-1}(z + p - 1)^{-p+1}$. Thus, the plot of $\log N(z) - \zeta$ is not linear, but the plot of $\log N(z) - \log(z + p - 1)$ becomes linear. Although TAMA300's data show non-Gaussian properties, these facts suggest that the $\log N(z) - \log(z + p - 1)$ plot may be more suitable for an accurate evaluation of the false alarm rate as a function of the threshold. We find that this is actually the case for DT8 and DT9. In Fig. 4, we show the result of the fitting for the DT9 case. The thresholds obtained in this way are listed in Table II. On the other hand, the same plot does not become linear in the DT6 case. We then conservatively select the region of the fitting so that we have a larger threshold for a given false alarm rate.
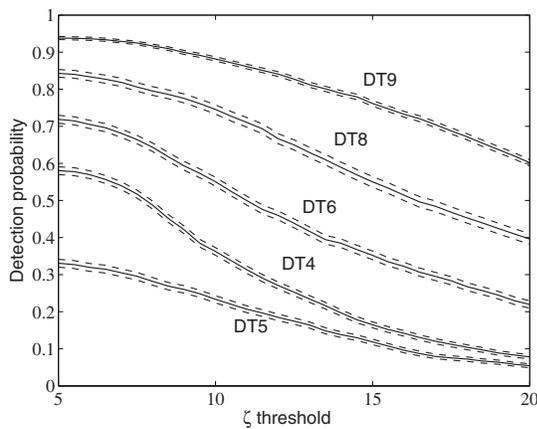

FIG. 3.   Detection probability of Galactic binaries inspirals for each observation run. The dashed lines show the uncertainty of the Monte Carlo simulations.
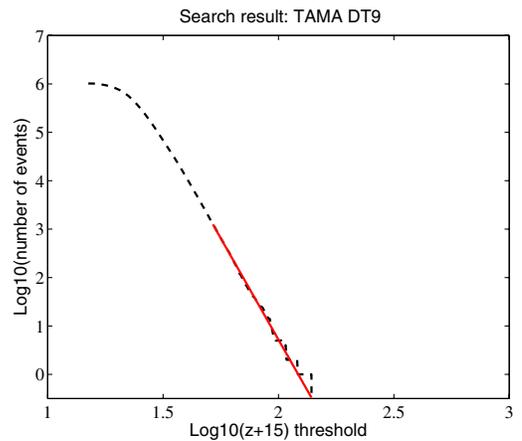

FIG. 4 (color online).   The dashed line denotes the cumulative number of triggers as a function of $\log_{10}(z + p - 1)$, $p = 16$, for DT9. The solid line is the result of the least square fitting to this trigger distribution.

TABLE II.   Summary of the upper limit on the Galactic event rate. The errors for the upper limit are evaluated in Sec. VI in detail.

	DT6	DT8	DT9
Observation time (hours)	876.6	1100	486.1
Threshold ζ^*	21.8	13.7	17.7
$N_{\mathrm{bg}}^{(i)}$	0.1000	0.1255	0.0555
Detection probability	0.18	0.60	0.69
$(\delta R_i)_{\mathrm{fluct}}$ (yr^{-1})	+20.6	+2.52	+4.04
	−24.0	−2.82	−3.77
$(\delta R_i)_{\mathrm{model}}$ (yr^{-1})	+55.4	+4.18	+6.84
	−16.6	−1.53	−2.60
R_i (yr^{-1})	130^{+59}_{-29}	$30^{+4.9}_{-4.6}$	$60^{+8.0}_{-4.6}$

TABLE III.   The various error sources and their values in the detection probability.

	DT6	DT8	DT9
Threshold	+0.001	+0.031	+0.013
	−0.000	−0.024	−0.022
Monte Carlo	±0.009	±0.014	±0.008
Calibration	+0.034	+0.045	+0.040
	−0.028	−0.041	−0.039
$(\delta\epsilon_i)_{\mathrm{fluct}}$	+0.035	+0.056	+0.042
	−0.029	−0.049	−0.045
Wave form	−0.028	−0.041	−0.039
Binary distribution model	±0.028	±0.032	±0.031
$(\delta\epsilon_i)_{\mathrm{model}}$	+0.028	+0.032	+0.031
	−0.056	−0.073	−0.070

With these thresholds, we have $N_{\mathrm{obs}}^{(i)} = 0$ for all cases. From Eq. (5.3), the upper limit on the number of events is $N_i = 2.3$ for a confidence level C.L. = 90%. We obtain the upper limit for the Galactic event rate, 130 (yr^{-1}) from DT6, 30 (yr^{-1}) from DT8, and 60 (yr^{-1}) from DT9. The thresholds, the detection probability, and the upper limit for the Galactic event rate for each run are listed in Table II. The most stringent upper limit is obtained from DT8 data. This is because the length of data is the longest among the three runs, and because the detection probability is comparable to that of DT9 on average.

We combine these results and obtain a single upper limit. The combined upper limit from different observation runs is given by

$$R = \frac{N_{\mathrm{UL}}}{\sum_i T_i \epsilon_i}, \qquad (5.4)$$

where N_{UL} is the upper limit on the number of events derived by all of the data. We adopt the same threshold ζ^* for each run listed in Table II. The total number of background triggers is $\sum_i N_{\mathrm{bg}}^{(i)} = 0.281$. Thus, we have 1 event per year as a false alarm rate for the combined DT6-DT8-DT9 data. Since the total number of triggers observed is zero, $\sum_i N_{\mathrm{obs}}^{(i)} = 0$, we have $N_{\mathrm{UL}} = 2.3$ for C.L. = 90%. From Eq. (5.4), the combined upper limit on the event rate becomes

$$R = 17 \ (\mathrm{yr}^{-1}). \qquad (5.5)$$

VI. STATISTICAL AND SYSTEMATIC ERRORS

We consider various error sources which affect the detection probability. These are summarized in Table III.

Threshold.—The method to derive the upper limit on the event rate in this paper requires the evaluation of the threshold which corresponds to a given false alarm rate. This is done by fitting the distribution of triggers as explained in Sec. V. There are statistical errors of the fitting

due to the fluctuation of the number of background triggers. These errors result in the error of the threshold, and the detection probability. We have the error of $-0.02 \sim +0.03$ in the detection probability in the DT8 and DT9 cases. In the DT6 case, as explained in Sec. V, the error of the fitting due to the nonlinear property of the distribution was already incorporated in the fitting. The statistical error of the fitting itself was very small in the DT6 case, $\lesssim 10^{-3}$.

Monte Carlo.—The error due to the Monte Carlo injection test with a limited trial number is given by $\sqrt{\epsilon_i(1 - \epsilon_i)/n_i}$, where n_i is the number of the Monte Carlo trials of each run. This Monte Carlo error becomes about ±0.01 in the detection probability.

Calibration.—The calibration of the sensitivity of TAMA300 is done by monitoring continuously the response of an injected sinusoidal test signal. The error of this response is much smaller than the normalization error described below, and can be neglected here. In the determination of the transfer function, there are two possible effects which affect the calibration uncertainty. One is an overall normalization error associated with the magnetic actuation strength uncertainty and its effect on calibration, and the other is the uncertainty in the frequency-dependent response. Although the error in the normalization is of order 5%, the long-term drift is unknown. We thus conservatively adopt 10%. The frequency-dependent error is known to be much less than 10%, and thus it is absorbed in the uncertainty in the normalization. The calibration uncertainty leads to errors of $-0.03 \sim +0.05$ in the detection probability. This calibration error is expected to depend on the different observation runs, and is expected to drift and/or fluctuate even within an observation run.

Binary distribution model.—We have adopted a specific model for the distribution of binary neutron stars in our Galaxy. If the distance between the Sun and the Galactic center is different from the adopted value, the detection probability will be changed. The uncertainty of this distance ±0.9 kpc leads to the uncertainty of the detection probability about ±0.03.

Wave form.—We used the wave form based on the 2.5 PN order. However, currently the best template has 3.5 PN order. The uncertainty of ρ due to this is at most 6%. However, it is reported that the PN wave form itself may contain uncertainty [19]. It is also reported that the restricted PN templates give overestimation on the signal-to-noise ratios compared to the more accurate, amplitude-corrected templates [20]. We thus adopt 10% reduction of the estimated ρ as an uncertainty. This produces an error of $-0.03 \sim -0.04$ in the detection probability.

The above errors propagate to the upper limit of the event rate for each run. We take a quadratic sum of the errors due to threshold, Monte Carlo injection test, and calibration, since they show the property of fluctuation, and since they are independent of each other. The sum of these errors, $(\delta\epsilon_i)_{\text{fluct}}$, is listed in Table III. The errors due to the binary distribution model and the theoretical wave form produce, simply, the shift of the detection probability. We thus take a linear sum of them conservatively. The sum of these errors, $(\delta\epsilon_i)_{\text{model}}$, is listed in Table III. We denote the effect of these errors to the upper limit for each run, R_i, as $(\delta R_i)_{\text{fluct}}$ and $(\delta R_i)_{\text{model}}$, respectively, which are shown in Table II. When we evaluate the total error for each run, we take a quadratic sum of $(\delta R_i)_{\text{fluct}}$ and $(\delta R_i)_{\text{model}}$, since they are independent of each other. As shown in Table II, the errors of the upper limit on the event rate for each run become $+59/-29$ (yr^{-1}) for DT6, $+4.9/-4.6$ (yr^{-1}) for DT8, and $+8.0/-4.6$ (yr^{-1}) for DT9.

Finally, we evaluate the error for the combined upper limit, Eq. (5.4). The effect of $(\delta\epsilon_i)_{\text{fluct}}$ on R is evaluated by taking a quadratic sum of each effect of $(\delta\epsilon_i)_{\text{fluct}}$ on R, and we have $+0.965/-1.08$ (yr^{-1}). The effect of $(\delta\epsilon_i)_{\text{model}}$ on R is evaluated by simply shifting each ϵ_i in Eq. (5.4), and we obtain $+2.86/-1.05$ (yr^{-1}). The total error in R is evaluated by taking a quadratic sum of these two errors. We have the upper limit with errors, $R = 17^{+3.02}_{-1.51}$ (yr^{-1}). By taking a larger value as a conservative upper limit, we obtain

$$R = 20 \ (\text{yr}^{-1}). \tag{6.1}$$

This value is much larger than an astrophysically expected value, 8.3×10^{-5} (yr^{-1}) [21], for the coalescence of neutron star binaries. However, this rate is smaller than that obtained by the LIGO S2 search, 47 $(\text{yr}^{-1}\text{MWEG}^{-1})$, or by the LIGO-TAMA joint analysis, 49 $(\text{yr}^{-1}\text{MWEG}^{-1})$. The main reason for this is that the length of data used in our analysis is much longer than in these analyses.

VII. SUMMARY AND DISCUSSION

In this paper, we have presented the results from the TAMA300 data analysis to search for gravitational waves from inspiraling compact binaries in a mass range $1M_\odot$–$3M_\odot$. We analyzed DT4, DT5, DT6, DT8, and DT9 data of TAMA300. There were no triggers which deviate from the tail of the distribution of triggers significantly. We thus conclude that there is no candidate trigger which can be interpreted as a real gravitational signal. By using the long and sensitive data from DT6, DT8, and DT9, we obtained upper limits on the Galactic event rate from each observation run. We combined these results and obtained a single upper limit, 20 (yr^{-1}), at a 90% confidence level from these three observation runs. We evaluated the systematic errors due to various effects such as the uncertainty of calibration and the uncertainty of the background estimation. In the upper limit, these effects were included.

The upper limit obtained in this paper is much larger than an astrophysically expected value for the coalescence of neutron star binaries. However, this upper limit is significant since it is derived by observation. Nevertheless, more sensitive detectors are necessary to obtain a more stringent upper limit on the event rate, and to detect the signal. TAMA300 is now improving the suspension system by installing the Seismic Attenuation System in order to obtain better sensitivity and better stability. When it is finished, it is expected to have much better sensitivity than DT9. LIGO has already performed 3rd and 4th science runs with better sensitivity than S2. Further, LIGO has now been conducting the 5th science run since November 2005, with its goal sensitivity. It can detect the inspiraling binaries up to a distance ~ 10 Mpc. It is expected to be able to set a much more stringent upper limit.

When the spin angular momentum of compact objects cannot be neglected, the spinless template is not good enough to detect the signal, and we need to employ templates with spins. However, since the number of parameters becomes much larger than in the nonspinning case, it requires very powerful computer resources. One way to avoid the use of the full templates with spins will be to use some phenomenological templates with a small number of parameters [22]. We will work on such cases in the future.

Despite the improvement and long-term observation of current detectors, the chance to detect gravitational waves by these first generation detectors will not be very large. We need more sensitive detectors, such as advanced LIGO [23] and LCGT [24]. These detectors will detect gravitational waves frequently, and will be used to investigate the strong field region of gravity and the astrophysics of compact objects.

[1] B. Willke *et al.*, Classical Quantum Gravity **21**, S417 (2004); H. Lück *et al.*, Classical Quantum Gravity **23**, S71 (2006).

[2] B. Abbott *et al.*, Nucl. Instrum. Methods **A517**, 154 (2004).

[3] M. Ando *et al.*, Phys. Rev. Lett. **86**, 3950 (2001); R. Takahashi *et al.*, Classical Quantum Gravity **21**, S403 (2004).

[4] F. Acernese *et al.*, Classical Quantum Gravity **21**, S385 (2004); **23**, S63 (2006).

[5] B. Allen *et al.*, Phys. Rev. Lett. **83**, 1498 (1999).

[6] H. Tagoshi *et al.*, Phys. Rev. D **63**, 062001 (2001).

[7] H. Takahashi *et al.*, Phys. Rev. D **70**, 042003 (2004).

[8] B. Abbott *et al.*, Phys. Rev. D **69**, 122001 (2004).

[9] B. Abbott *et al.*, Phys. Rev. D **72**, 082001 (2005).

[10] B. Abbott *et al.*, Phys. Rev. D **72**, 082002 (2005).

[11] B. Abbott *et al.*, Phys. Rev. D **73**, 062001 (2006).

[12] S. Fairhurst and H. Takahashi, Classical Quantum Gravity **22**, S1109 (2005); B. Abbott *et al.* (LIGO Scientific Collaboration and TAMA Collaboration), Phys. Rev. D **73**, 102002 (2006).

[13] H. Takahashi *et al.*, Classical Quantum Gravity **21**, S697 (2004).

[14] L. Blanchet, G. Faye, B. R. Iyer, and B. Joguet, Phys. Rev. D **65**, 061501(R) (2002); L. Blanchet, B. R. Iyer, and B. Joguet, Phys. Rev. D **65**, 064005 (2002).

[15] B. J. Owen, Phys. Rev. D **53**, 6749 (1996); B. J. Owen and B. S. Sathyaprakash, Phys. Rev. D **60**, 022002 (1999).

[16] T. Tanaka and H. Tagoshi, Phys. Rev. D **62**, 082001 (2000).

[17] B. Allen, Phys. Rev. D **71**, 062001 (2005).

[18] This χ^2 means the reduced chi square, which is the usual chi square divided by the degree of freedom. In this paper, the number of bins of the frequency region is taken to be 16. Thus, the degree of freedom of χ^2 is 30.

[19] S. Droz and E. Poisson, Phys. Rev. D **56**, 4449 (1997); S. Droz, Phys. Rev. D **59**, 064030 (1999).

[20] C. Van Den Broeck and A. S. Sengupta, Classical Quantum Gravity **24**, 155 (2007).

[21] V. Kalogera *et al.*, Astrophys. J. **601**, L179 (2004); **614**, L137(E) (2004).

[22] A. Buonanno, Y. Chen, and M. Vallisneri, Phys. Rev. D **67**, 104025 (2003).

[23] P. Fritschel, in *Astrophysical Sources for Ground Based Gravitational Wave Detectors*, edited by J. M. Centrella, AIP Conf. Proc. No. 575 (AIP, New York, 2001), pp. 15–23.

[24] K. Kuroda, Classical Quantum Gravity **23**, S215 (2006).